cambridge.org/aog

Interpreting englacial layer deformation in the presence of complex ice flow history with synthetic radargrams

Cooper W. Elsworth[1] [iD], Dustin M. Schroeder[1,2] and Matthew R. Siegfried[1,3] [iD]

[1]Department of Geophysics, Stanford University, Stanford, CA, USA; [2]Department of Electrical Engineering, Stanford University, Stanford, CA, USA and [3]Department of Geophysics, Colorado School of Mines, Golden, CO, USA

Abstract

Fast ice flow on the Antarctic continent constitutes much of the mass loss from the ice sheet. However, geophysical methods struggle to constrain ice flow history at depth, or separate the signatures of topography, ice dynamics and basal conditions on layer structure. We develop and demonstrate a methodology to compare layer signatures in multiple airborne radar transects in order to characterize ice flow at depth, or improve coverage of existing radar surveys. We apply this technique to generate synthetic, along-flow radargrams and compare different deformation regimes to observed radargram structure. Specifically, we investigate flow around the central sticky spot of Whillans Ice Stream, West Antarctica. Our study suggests that present-day velocity flowlines are insufficient to characterize flow at depth as expressed in layer geometry, and streaklines provide a better characterization of flow around a basal sticky spot. For Whillans Ice Stream, this suggests that ice flow wraps around the central sticky spot, supported by idealized flow simulations. While tracking isochrone translation and rotation across survey lines is complex, we demonstrate that our approach to combine radargram interpretation and modeling can reveal critical details of past ice flow.

Introduction

Ice streams and outlet glaciers account for the majority of ice loss from the Antarctic ice sheet (e.g. Bamber and others, 2000; Rignot and others, 2019), but observational data are limited by a short observational period and inherent difficulty in viewing the subsurface. The primary technique to efficiently probe the glacial subsurface at large spatial scales is airborne radio-echo sounding (e.g. Evans and others, 2004; Chu and others, 2016; Jordan and others, 2017), which leverages the transparency of ice to specific electromagnetic frequencies. Since the 1960s (Evans and Smith, 1970), airborne radar has been used to image large swaths of the Greenland and Antarctic ice sheets. These airborne surveys record the depth-varying return of electromagnetic waves reflected by englacial reflective layers, interpreted as isochrones (i.e. layers of snow deposited at the same time; e.g. Eisen and others, 2008; Grima and others, 2014; Cavitte and others, 2018). Specifically, transmitted radio waves scatter due to variations in dielectric properties between isochronal layers, generating an image of the ice column.

Isochrones have long provided insights into ice-sheet history, due to the extended timescale that they record (e.g. Hudleston, 2015; Macgregor and others, 2016). These layers are passively advected with flow, recording cumulative deformation of the ice mass (e.g. Ng and Conway, 2004; Siegert and others, 2013; Bingham and others, 2015; Winter and others, 2015; Bons and others, 2016; Young and others, 2018). Isochrones have been interpreted as tracers at ice divides to confirm theoretical ice deformation mechanisms in a relatively simple deformational regime (Raymond, 1983; Vaughan and others, 1999). Similarly, in instances where radargrams exactly follow ice flowlines, paleo-reconstructions and steady-state imprints of isochrone deformation have been demonstrated (Wolovick and others, 2014; Gudlaugsson and others, 2016; Wolovick and Creyts, 2016; Holschuh and others, 2017). However, large deformations in the ice column make it challenging to reliably infer the past flow history from radar sounding interpretations.

A major issue with interpreting isochrones as a proxy for dynamics is the limited coverage of radar transects, compared to the deformational regime in many areas of the ice sheets. At an ice divide where flow is pseudo-2-D, out-of-plane deformation can be neglected and the interpretation is relatively straightforward (e.g. Raymond, 1996; Nereson and others, 1998; Conway and Rasmussen, 2009). However, in regions where the flow is complex or the radar transects are not aligned with the flow axis, out-of-plane deformation can confound interpretation (e.g. Vieli and others, 2007; Siegert and others, 2013; Bons and others, 2016). A salient example of complex flow are Antarctic ice streams (i.e. regions of fast ice flow), where our understanding of ice flow limits our understanding of overall ice-sheet mass loss. The influence of basal resistance on isochrone deformation has been shown along flowlines (Wolovick and others, 2014; Gudlaugsson and others, 2016; Wolovick and Creyts, 2016; Holschuh and others, 2017), but a method has not been developed to compare radar profiles of arbitrary orientation. Many studies interpret isochrone deformation as paleo-ice flow without methods to quantify the
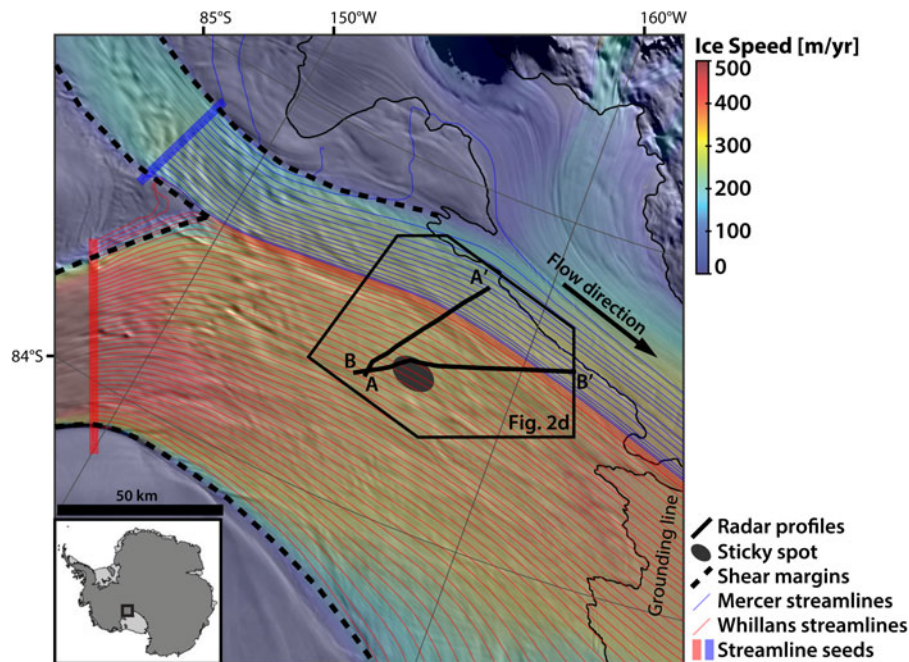
Fig. 1. Map of the study area colored by surface velocity (Rignot and others, 2017), showing the stream-lines from Whillans (red) and Mercer (blue) IceStreams, and the ASAID grounding line (Bindschadler and others, 2011). Map was generated with the Antarctic Mapping Toolbox (Greene and others, 2017).

conclusions (Ng and Conway, 2004; Christianson and others, 2013; Siegert and others, 2013; Keisling and others, 2014; Bingham and others, 2015; Winter and others, 2015; Bons and others, 2016). Alternatively, theoretical studies have developed isochrone advection as tracers in large-scale ice-sheet models (Born, 2017; Clarke and others, 2005; Hindmarsh and others, 2006). An alternative methodology is necessary to confirm to observational interpretations in regions of complex flow. Moreover, the limited coverage of radar surveys motivates resampling of an existing survey along a profile of interest (e.g. a flowline), or in locations where other field data have been collected.

A benchmark setting of particular interest is flow over and around a basal sticky spot. In regions where ice flow is facilitated by a weak, failing bed, sticky spots are areas with anomalously high basal resistance. They were first identified by the warping and generation of streaklines on the ice surface, and subsequently studied as specific examples of basal conditions (e.g. Stokes and others, 2007; Sergienko and Hulbe, 2011). Observationally, sticky spots have been imaged from the surface through seismic surveys (e.g.Winberry and others, 2011; Luthra and others, 2016, 2017). These anomalous patches provide much higher basal resistance than the surrounding region and therefore are thought to resist the majority of ice flow (Alley, 1993; Anandakrishnan and Alley, 1994; MacAyeal and others, 1995; Joughin and others, 2002; Price and others, 2002; Joughin and others, 2004), compensating for up to 13% of the driving stress for some ice streams (Alley, 1993). The locations and role of sticky spots are therefore an important consideration in characterizing mass loss from the ice sheets.

Characterizing the flow over a sticky spot is confounded by the relatively short timescale of the observational record. Present-day velocity maps provide a snapshot of the extent and magnitude of fast ice flow in amazing detail (Rignot and others, 2011, 2017). Streamlines are the paths of passively advected parcels in the present-day flow field. Alternatively, features called streaklines, or 'flow stripes', represent short wavelength surface roughness associated with streaming flow (Bindschadler and Vornberger, 1998). Streaklines are thought to record past ice flow history over an irregular bed (Fahnestock and others, 2000). The connection between streamlines, streaklines, and internal stratigraphy remains unclear, with studies demonstrating that isochrone

folds lack correspondence to surface streaklines (Campbell and others, 2008).

In this paper, we consider the flow and deformation of isochrones around the central sticky spot of Whillans Ice Stream, shown in Figure 1. This sticky spot is the initiation point of stick-slip events that facilitate the large-scale motion of the ice stream (e.g. Winberry and others, 2011; Lipovsky and Dunham, 2017; Barcheck and others, 2018). Active and passive seismic surveys have been deployed to characterize the location of this stick-slip patch (e.g. Winberry and others, 2011; Barcheck and others, 2018) and determine the properties of the bed (e.g. Luthra and others, 2016). However, the timescale over which the sticky spot has been active and the size of the sticky spot remain unknown. Luthra and others (2016) found that the sticky spot is likely due to a local topographic high in the bedrock, diverting subglacial meltwater from this region. We consider the along-flow deformation of internal layers over the Whillans central sticky spot and develop a method to generate synthetic radargrams along flow. Specifically, we compare radar features between upstream and downstream radar profiles over the Whillans central sticky spot to place observational constraints on flow history. By considering englacial layers, deformation can be inferred throughout the ice column, compared to only observing streaklines at the surface (Fahnestock and others, 2000; Hulbe and Fahnestock, 2007; Glasser and Gudmundsson, 2012; Roberts and others, 2013).

We demonstrate that the deformation of internal layers suggests flow diversion around the sticky spot, following surface streaklines. The length scale over which this deformation occurs suggests this basal sticky spot has been active for centuries. Based on our synthetic radargrams, we identify distinct features that propagate undistorted for kilometers along flow. This confirms that a well-lubricated bed supports Whillans Ice Stream and basal slip, u_b, dominates the velocity profile. These results are consistent with the use of a Shelfy-Stream model for ice stream trunks (MacAyeal, 1989). From the streakline displacements and idealized modeling, we estimate the size of the sticky spot to cover a larger area than the stick-slip patch determined by active and passive surveying. This analysis underscores the complexity of isochrone interpretation, with isochrone rotation and translation occurring across radargrams.

Methods

We develop a methodology to construct synthetic radargrams in regions of fast-flowing ice. This method employs certain assumptions in this implementation, and we refer to it as the Synthetic Advected Radargram Algorithm.

Model assumptions

Regions of fast flowing ice are often facilitated by a weak underlying bed (e.g. Tulaczyk and others, 2000). Basal strength inversions for many ice streams indicate that the bed supports nearly none of the driving stress (Joughin and others, 2002, 2004; Cuffey and Patterson, 2010). Therefore, we can consider the analytical solution of ice speed with depth, z,

$$u(z) = u_{\text{b}} + u_{\text{e}}, \tag{1}$$

$$= u_{\text{b}}(\tau_{\text{c}}, N, p) + \frac{2A}{n+1} \tau_{\text{b}}^n H\left(1 - \left(1 - \frac{z}{H}\right)^{n+1}\right), \tag{2}$$

with basal velocity, u_{b}, englacial deformation, u_{e}, flow-law prefactor, A, flow-law power, n, basal shear stress, τ_{b} and ice column height, H (Cuffey and Patterson, 2010). Basal velocity in regions with failing, weak, unconsolidated till is a function of basal yield strength, τ_{c}, normal stress, N and pore pressure, p (Tulaczyk and others, 2000). For regions of fast flow, basal shear stress is very small ($\tau_{\text{b}} \rightarrow 0$) and basal velocity dominates englacial deformation in the ice column ($u_{\text{b}} \gg u_{\text{e}}$). Despite the local influence of sticky spots, fast-flowing ice streams are generally considered to follow the physics of a 'Shelfy-Stream' model (MacAyeal, 1989; Joughin and others, 2004). If we consider the sticky spot to be a transient feature that slows down most of the ice column as a unit, basal velocity dominates and we can assume that englacial deformation is negligible ($u_{\text{b}} \gg u_{\text{e}}$). We therefore argue that our radargrams are passively transported along flow, uniform with depth. While this assumption may not be valid in all settings, this assumption will be tested in this analysis.

Methodology

To generate synthetic radargrams, we develop a technique to sample an advected radargram along an alternative acquisition line, using the assumption of negligible ice column deformation. As shown in Figure 2a, this method requires one radargram upstream (Profile A), a downstream profile of interest (Profile B) and a hypothesized map-view flow field, $\mathbf{u}(x, y)$ (variations with depth, z, are neglected). Profile A can then be passively transported along the flow field by a given spatial step size, $\Delta x_{\parallel}$, and sampled with bilinear interpolation where Profile A intersects Profile B, shown as magenta dots. The spatial coordinates of Profile A, $\mathbf{x}$, are advected using Euler integration,

$$\mathbf{x}_{i+1} = \mathbf{x}_i + \Delta x_{\parallel} \frac{\mathbf{u}(\mathbf{x}_i)}{|\mathbf{u}(\mathbf{x}_i)|}, \tag{3}$$

with sufficiently small step size, $\Delta x_{\parallel}$, less than the along track resolution of the Profile A radargram. The sampling of the return power of Profile A onto the synthetic radargram of Profile B is computed with bilinear interpolation of the four nearest values of Profile A. By sampling and storing the interpolated values of Profile A along Profile B, we return a synthetic radargram that would be generated by the hypothesized flow field, shown as the dashed magenta line in Figure 2a. A link to a well-commented version of the code is included in the Acknowledgements for ease of use and modification.
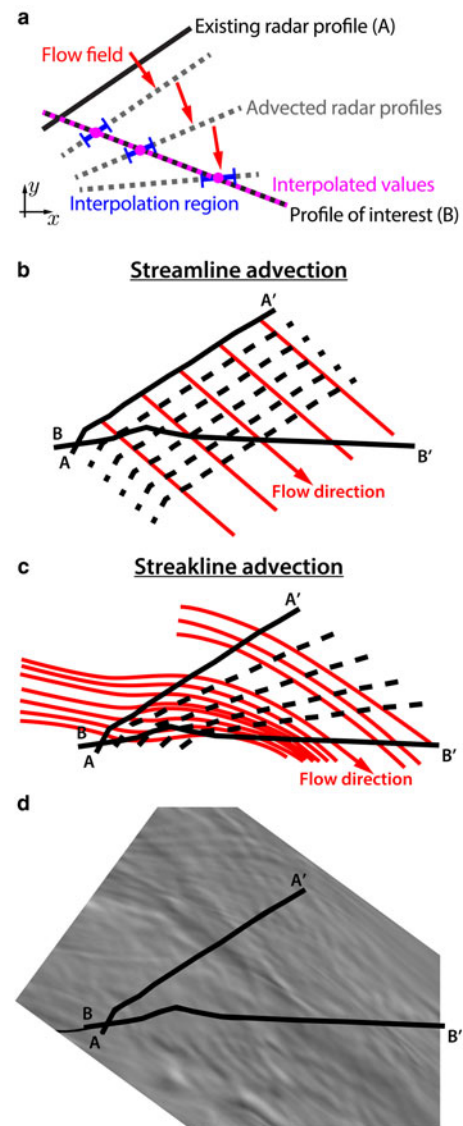

Fig. 2. (a) Schematic of the synthetic radargram generation algorithm. An existing radar profile is resampled onto another profile line (black), given a vector flow field (red). The position of the advected radar profiles (gray dash) are computed along the length of the profile of interest. Interpolation is performed only on a local region for computational efficiency, and the interpolations are computed in parallel. The result is a synthetic radargram (magenta dash) generated along the profile of interest. (b), (c) The two ice flow hypotheses for the Whillans central sticky spot are flow along current surface velocity streamlines (b), and along surface streaklines derived from MODIS (c). (d) MODIS imagery of streaklines on Whillans Ice Stream (Scambos and others, 2007).

While this technique works conceptually, in practice the along-track resolution of the radargrams is prohibitive for this technique to be computationally feasible over multi-kilometer length scales. Therefore, we introduce efficiency improvements to make the synthetic radargram generation tractable for real applications. The most costly component of this technique is interpolation from the advected radargram to the synthetic radargram at each spatial step. By reducing the number of points to search for the nearest neighbors, we can improve the runtime dramatically. We achieve this by considering only points in Profile A that are a distance, $\Delta x_{\perp}$, or closer to Profile B at a given spatial step (shown as the blue region in Fig. 2a), thereby reducing the search and interpolation times dramatically. To pre-compute the number of computational steps performed during the advection of Profile A, a search along the advected path of Profile A is performed to output the first and last positions where Profile A intersects Profile B. Finally, this algorithm does not require information from
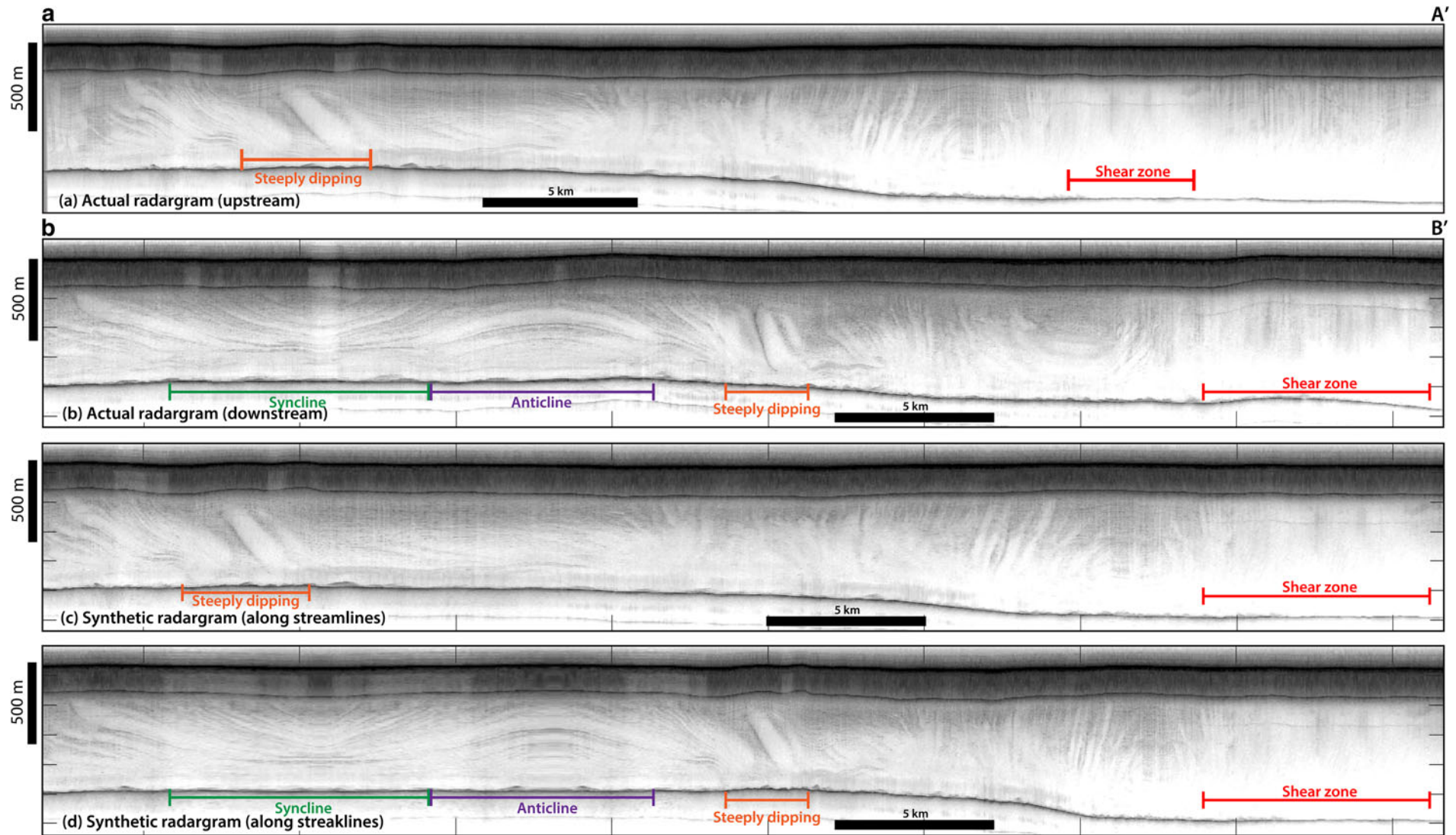
Fig. 3. Radargrams (a) upstream and (b) downstream of the Whillans central sticky spot. The downstream radargram shows complex deformation that is not easily interpreted by intuition alone. (c) A synthetic downstream radargram generated using present-day velocity streamlines. This synthetic radargram does not reproduce many of the features in the observed downstream radargram. (d) A synthetic downstream radargram generated using surface streaklines and matched englacial features. This radargram is able to reproduce nearly all of the englacial features in the observed downstream radargram.

prior spatial steps to compute the interpolation at a given spatial step (i.e. an 'embarrassingly parallel' algorithm). Therefore, we implement this method in parallel by splitting the interpolation of advected profiles across processors. Each segment of the synthetic radargram is generated separately, and the entire synthetic radargram is concatenated as a final processing step.

Field setting and data

To contrast the behavior of ice at depth to surface observables, we consider the information provided by both velocity streamlines and surface streaklines (Glasser and Gudmundsson, 2012). Velocity streamlines (Fig. 1) are derived by tracking the path of a parcel of ice through satellite-derived surface velocity estimates (Rignot and others, 2011). These streamlines are generated by advecting particles along the modern surface velocity field, again using the Euler integration (Eqn (3)). In the trunk of Whillans Ice Stream, the plug-like flow profile enables a uniform velocity field, leading to parallel, uniform streamlines (Fig. 2b). In contrast, streaklines are an indicator of past flow history, being generated by basal asperities in the paleo-flow field and maintained as surface topographic expressions (Fahnestock and others, 2000; Hulbe and Fahnestock, 2007; Glasser and Gudmundsson, 2012; Roberts and others, 2013). Streaklines can be easily seen in MODIS imagery of the region (Scambos and others, 2007), and wrap around the sticky spot (Fig. 2c).

In this analysis, we consider two airborne radar profiles collected by the Center for Remote Sensing of Ice Sheets during 2013–2014 field season using the Multi-Channel Coherent Radar Depth Sounder (MCoRDS) radar system (Shi and others, 2010). We consider only the high-gain channel of the MCoRDS L1B data product for imaging the deep ice layers at depth. The radar data were collected with the MCoRDS 2 radar system using a transmit power of 1500 W and bandwidth of 180–210 MHz (Shi and others, 2010). Specifically, we consider two radar profiles collected over Whillans Ice Stream: one upstream and one downstream of the sticky spot (Fig. 1). The structure of the radargrams suggest a complex flow history imprinted into the isochrones (Fig. 3). The upstream profile (Fig. 3a) contains many regions with steeply dipping layers, characterized by the linear features, which lack clear reflections (Holschuh and others, 2014). Ice advected from the suture zone where Whillans and Mercer Ice Streams merge lacks any clear internal reflectors. This is likely a result of the highly deformed ice distorting the isochrones to such an extent that they become destroyed, and indistinguishable in radar returns. The downstream profile (Fig. 3b) exhibits many complex flow features including large anticlines, synclines, steeply dipping layers and destroyed layers from the Whillans–Mercer suture zone. The interpretation of these features is difficult, and verification of an interpretation is even more challenging. Applying our methodology to these compelling radargrams allows for a quantitative comparison of disparate flow hypotheses over the Whillans central sticky spot.

Results

We apply the Synthetic Advected Radargram Algorithm to sample the advection of Profile A along Profile B, across the central sticky spot of Whillans Ice Stream. First, we consider the case where Profile A follows present-day streamlines, with the synthetic radargram shown in Figure 3c. Comparing the synthetic radargram to the actual radargram across Profile B, we find that the synthetic radargram does not reproduce many of the complex isochrone structural features. It matches the location and width of the suture zone, but the steeply dipping layers occur in the wrong position. Moreover, it does not reproduce the anticline and syncline features of the actual radargram. Second,
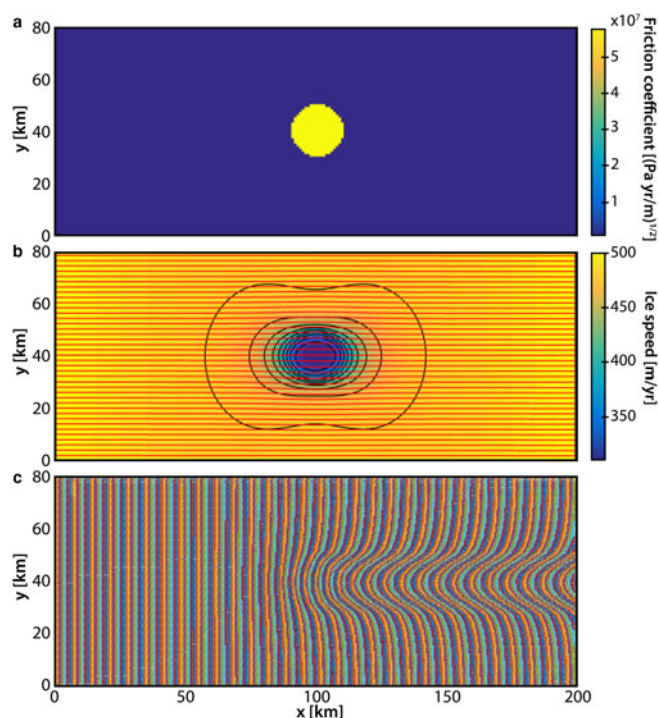

Fig. 4. Simulation of flow over an idealized sticky spot. (a) Uniform basal friction coefficient across the domain, with a centered, abrupt, circular sticky spot. (b) Flow field computed by ISSM, colored by ice speed, and showing streamlines (red). The streamlines do not noticeably deviate from parallel to driving stress. (c) Particles introduced to the flow at x=0, colored by their introduction time, and advected through the steady-state flow field. There is a distinct rotation and wrapping of the advected particles across the sticky spot, which matches the interpretation of the advected radargrams.

we consider the case where Profile A is advected downstream along surface streakline paths, with the synthetic radargram shown in Figure 3d. Comparing this synthetic radargram to the actual radargram, shows that many of the complex structural features are reproduced in great detail. This deformational hypothesis recovers the location and widths of the anticline, syncline, steeply dipping layers and suture zone.

Analysis

To better understand these disparate flow hypotheses, we conduct an idealized modeling study of flow over a sticky spot in the Ice Sheet System Model (ISSM) (Larour and others, 2012). The model is an idealized (rectangular) ice stream, described by the Shelfy-Stream Approximation (e.g. Morland, 1987; MacAyeal, 1989; Bueler and Brown, 2009), with a central, circular sticky spot of anomalously high friction coefficient (Fig. 4a). Tuning the ratio of the friction coefficient and driving stress reproduces velocities similar to the trunk of Whillans Ice Stream (Fig. 4b). Despite a pronounced deceleration of ice flow over the sticky spot, the ice streamlines are not noticeably skewed by the sticky spot, and rather stay parallel to the driving stress. Alternatively, we can advect particles through the velocity field in the same way that englacial ice would experience advection, analogous to radargram advection (Fig. 4c). The advected particles experience a distinct rotation and wrapping around the sticky spot, similar to the streakline flow hypothesis. This idealized case demonstrates that these two flow hypotheses are not conflicting, instead streaklines store a more nuanced view of ice flow compared to streamlines.

Therefore, this analysis suggests that a paleo-flow field similar to surface streaklines persists at depth. It also demonstrates that the assumption that negligible deformation exists in this part of
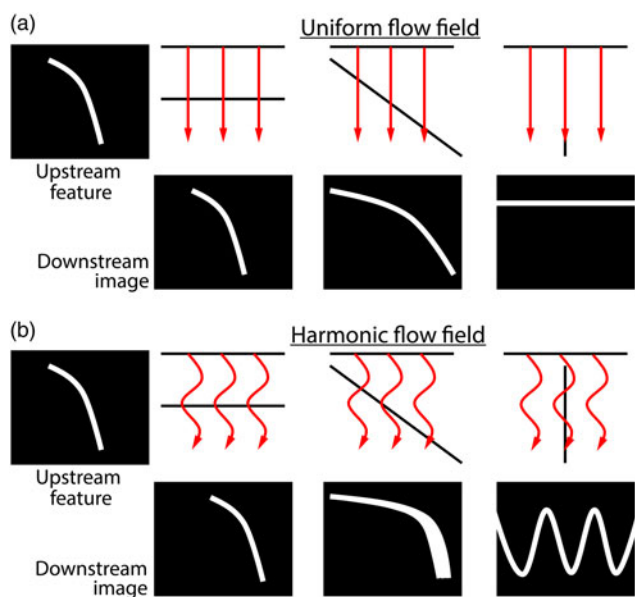
Fig. 5. Applications of this technique include verifying dynamic interpretations of isochrone structure, and resampling an existing survey. (a) Deformation and imaging of a dipping isochrone in different flow regimes. In a relatively simple (linear) deformational setting, obliquity of a radar transect result in an intuitive compression of a radar feature. In a slightly more complex (harmonic) deformational setting, obliquity of radar transects result in less intuitive imaging of an advected radar feature. (b) Resampling an existing radar survey is useful for analysis in cases where the existing survey geometry is not ideal. This includes resampling along a flowline or resampling a survey to allow for comparisons to other field measurements.

the ice column is valid. In this region, isochrone features persist over tens of kilometers in the ice stream trunk.

Discussion

In regions of fast flow, synthetic radargrams can reproduce complex features in the ice column, and supply observational constraints for paleo-flow hypotheses. This analysis demonstrates that isochrone advection can provide additional information of flow history at depth, in conjunction with surface streaklines (Fahnestock and others, 2000; Hulbe and Fahnestock, 2007; Glasser and Gudmundsson, 2012; Roberts and others, 2013). In contrast to the results of Campbell and others (2008), these results suggest that isochronal deformation corresponds to the paths defined by surface streaklines. This may be a matter of scale, as this study considers only a portion of the ice stream trunk, not the entire length. This discrepancy cautions the use of this methodology for longer spatial scales. Additionally, the advected and re-sampled basal reflector is not physical, and should not be interpreted as real.

Our analysis also underscores the limitations of isochrone interpretation in regions of fast flow. In regions where radargrams are not aligned with ice flowlines, out-of-plane deformation adds complexity to the interpretation of flow history. Even in this study area, where flow around a sticky spot is relatively straightforward, the observed features (Fig. 3b) are unintuitive without a method to validate interpretation. Synthetic radargrams are therefore an enabling tool to provide testing of flow history hypotheses in regions with multiple radargrams along flow.

This analysis illustrates how large anticline and syncline features can be generated by the out-of-plane advection of features across a radargram (Fig. 5). The steeply dipping layers in Profile A are advected across the plane of Profile B, generating the distinct anticline and syncline features. Figure 5a illustrates that when an upstream feature is advected downstream in a simple (linear) deformational setting, the angle, or obliquity, with which the radar transect crosses flow results in an intuitive expansion of

the radar feature. However, in a slightly more complex (harmonic) deformational setting, Figure 5b, the obliquity of the radar transect results in a distinctly different image of a downstream advected radar feature.

The method we have developed will hold for arbitrary 3-D flow fields, $\mathbf{u}(x, y, z)$. This includes situations where the bed is not weak and there is internal deformation in the ice column ($u_b \gg u_e$), as in Eqns (1–2). Using a 3-D flow field, the evolution equation described by Eqn (3), still holds for a 3-D implementation. Using depth-varying velocity, the radargram will distort as it is advected through the sampling profile. Sampling of the advected domain may be confounded by the domain passing out of the sampling region. In practice, a suitable 3-D flow field must be generated, such as with a higher-order ice-sheet model (Pattyn, 2003; Pattyn and others, 2008). The output of ice-sheet models could be validated by using their velocity fields to generate synthetic radargrams and comparing to observations. As with the 2-D implementation, the bed geometry of the synthetic radargrams is not physical, and not interpretable.

For this application, further quantification of uncertainty would be beneficial to provide a metric to validate models. One possibility is to use methods developed in image processing to quantify the similarity of the synthetic radargram to the observed radargram (e.g. Chopra and others,). This might provide a more quantitative comparison of flow hypotheses. Additionally, a quantitative similarity metric could be used an objective function in an inverse model to tune an unknown flow field in a region of interest. The inverse approach would allow a model to tune the velocity field in a 3-D sense across the entire ice column, in contrast to hypotheses informed solely by surface observations. Quantitative metrics of image similarity are still in a nascent state of research, therefore this is beyond the current scope of this methodology.

Another application of this method, separate from hypothesis testing, assumes that the flow field in a region is well constrained. In this case, the input flow field is the known quantity, and existing radar surveys can be resampled along profiles of interest. This technique could resample radar surveys along flowlines, improve the coverage of existing surveysor resample radar profiles where other field data were collected to provide additional, direct context for field experiments. This technique would need to be applied carefully, as it might only be appropriate at a local scale. However, this study demonstrates that in regions underlain by flat, weak beds, radargrams can advect in a meaningful way over tens of kilometers. Applying this methodology in regions with more basal heterogeneity would require further analysis. Promising features that could be resampled across surveys are image-obstructing diffractors (Catania and Neumann, 2010) or steeply dipping layers (Holschuh and others, 2014).

Conclusions

We developed a method to resample radargrams in regions of fast flow, and provided some insights into isochrone deformation at depth. Specifically, our technique allowed us to compare seemingly disparate flow hypotheses across the central sticky spot of Whillans Ice Stream. Our analysis provided a direct visual comparison between the hypothesized flow regimes for this region, by comparing synthetic radargrams to actual radargrams acquired in the region. We found that flow along surface streaklines persists at depth, and provided a better description of past flow history, compared to present-day surface velocity streamlines. Overall, our study provides a quantitative method to test interpretation of isochrone structure, and a potential avenue for resampling existing surveys in regions with well-constrained flow.

References

Alley RB (1993) In search of ice-stream sticky spots. *Journal of Glaciology* **39** (133), 447–454.

Anandakrishnan S and Alley RB (1994) Ice Stream C, Antarctica, sticky spots detected by microearthquake monitoring. *Annals of Glaciology* **20**, 183–186.

Bamber JL, Vaughan DG and Joughin I (2000) Widespread complex flow in the interior of the Antarctic ice sheet. *Science (New York, N.Y.)* **287**(5456), 1248–1250.

Barcheck CG, Tulaczyk S, Schwartz SY, Walter JI and Winberry JP (2018) Implications of basal micro-earthquakes and tremor for ice stream mechanics: Stick-slip basal sliding and till erosion. *Earth and Planetary Science Letters* **486**, 54–60.

Bindschadler R and Vornberger PL (1998) Changes in the West Antarctic Ice Sheet since 1963 from declassified satellite photography. *Science (New York, N.Y.)* **279**(5351), 689–692.

Bindschadler R and 17 others (2011) Getting around Antarctica: new high-resolution mappings of the grounded and freely-floating boundaries of the Antarctic ice sheet created for the International Polar Year. *The Cryosphere* **5**, 569–588.

Bingham RG and 5 others (2015) Ice-flow structure and ice dynamic changes in the Weddell Sea sector of West Antarctica from radar-imaged internal layering. *Journal of Geophysical Research: Earth Surface* **120**(4), 655–670.

Bons PD and 10 others (2016) Converging flow and anisotropy cause large-scale folding in Greenland's ice sheet. *Nature Communications* **7**, 11427.

Born A (2017) Tracer transport in an isochronal ice-sheet model. *Journal of Glaciology* **63**(237), 22–38.

Bueler E and Brown J (2009) Shallow shelf approximation as a 'sliding law' in a thermomechanically coupled ice sheet model. *Journal of Geophysical Research: Solid Earth* **114**(3), 1–21.

Campbell I, Jacobel R, Welch B and Pettersson R (2008) The evolution of surface flow stripes and stratigraphic folds within Kamb Ice Stream: why don't they match?. *Journal of Glaciology* **54**(186), 421–427.

Catania GA and Neumann T (2010) Persistent englacial drainage features in the Greenland ice sheet. *Geophysical Research Letters* **37**(2), 1–5.

Cavitte MG and 7 others (2018) Accumulation patterns around Dome C, East Antarctica, in the last 73 kyr. *Cryosphere* **12**(4), 1401–1414.

Chopra S, Hadsell R and LeCun Y (2005) Learning a similarity metric discriminatively, with application to face verification. IEEE Computer Vision and Pattern Recognition (CVPR) Conference, pp. 539–546.

Christianson K and 8 others (2013) Ice sheet grounding zone stabilization due to till compaction. *Geophysical Research Letters* **40**(20), 5406–5411.

Chu W and 5 others (2016) Extensive winter subglacial water storage beneath the Greenland Ice Sheet. *Geophysical Research Letters* **43**(24), 484–492.

Clarke GK, Lhomme N and Marshall SJ (2005) Tracer transport in the Greenland ice sheet: three-dimensional isotopic stratigraphy. *Quaternary Science Reviews* **24**(1–2), 155–171.

Conway H and Rasmussen L (2009) Recent thinning and migration of the Western Divide, Central West Antarctica. *Geophysical Research Letters* **36** (12), 1–5.

Cuffey KM and Patterson WSB (2010) *The Physics of Glaciers*, **volume 2**, Burlington, MA: Butterworth-Heinemann, imprint of Elsevier.

Eisen O and 15 others (2008) Ground-based measurements of spatial and temporal variability of snow accumulation in East Antarctica. *Reviews of Geophysics* **46**(2), 1–39.

Evans J, Dowdeswell JA and Cofaigh CÓ (2004) Late quaternary submarine bedforms and ice-sheet flow in Gerlache Strait and on the adjacent continental shelf, Antarctic Peninsula. *Journal of Quaternary Science* **19** (4), 397–407.

Evans S and Smith B (1970) Radio echo exploration of the Antarctic ice sheet, 1969–70. *Polar Record* **15**(96), 336–338.

Fahnestock MA, Scambos TA, Bindschadler RA and Kvaran G (2000) A millennium of variable ice flow recorded by the Ross Ice Shelf, Antarctica. *Journal of Glaciology* **46**(155), 652–664.

Glasser NF and Gudmundsson H (2012) Longitudinal surface structures (flowstripes) on Antarctic glaciers. *The Cryosphere* **6**(2), 383–391.

Greene CA, Gwyther DE and Blankenship DD (2017) Antarctic mapping tools for MATLAB. *Computers and Geosciences* **104**, 151–157.

Grima C, Blankenship DD, Young DA and Schroeder DM (2014) Surface slope control on firn density at Thwaites Glacier, West Antarctica: results from airborne radar sounding. *Geophysical Research Letters* **41**(19), 6787–6794.

Gudlaugsson E, Humbert A, Kleiner T, Kohler J and Andreassen K (2016) The influence of a model subglacial lake on ice dynamics and internal layering. *The Cryosphere* **10**(2), 751–760.

Hindmarsh RC, Leysinger Vieli GJM, Raymond MJ and Gudmundsson GH (2006) Draping or overriding: the effect of horizontal stress gradients on internal layer architecture in ice sheets. *Journal of Geophysical Research: Earth Surface* **111**(F2), 1–17.

Holschuh N, Christianson K and Anandakrishnan S (2014) Power loss in dipping internal reflectors, imaged using ice-penetrating radar. *Annals of Glaciology* **55**(67), 49–56.

Holschuh N, Parizek BR, Alley RB and Anandakrishnan S (2017) Decoding ice sheet behavior using englacial layer slopes. *Geophysical Research Letters* **44**(11), 5561–5570.

Hudleston PJ (2015) Structures and fabrics in glacial ice: a review. *Journal of Structural Geology* **81**, 1–27.

Hulbe C and Fahnestock M (2007) Century-scale discharge stagnation and reactivation of the Ross ice streams, West Antarctica. *Journal of Geophysical Research* **112**(F3), F0327.

Jordan TM and 6 others (2017) Self-affine subglacial roughness: consequences for radar scattering and basal water discrimination in northern Greenland. *The Cryosphere* **11**(3), 1247.

Joughin I, MacAyeal DR and Tulaczyk S (2004) Basal shear stress of the Ross ice streams from control method inversions. *Journal of Geophysical Research* **109**(B9), 1–20.

Joughin I, Tulaczyk S, Bindschadler R and Price SF (2002) Changes in West Antarctic ice stream velocities: observation and analysis. *Journal of Geophysical Research: Solid Earth* **107**(B11), EPM–3.

Keisling Ba and 8 others (2014) Basal conditions and ice dynamics inferred from radar-derived internal stratigraphy of the northeast Greenland ice stream. *Annals of Glaciology* **55**(67), 127–137.

Larour E, Seroussi H, Morlighem M and Rignot E (2012) Continental scale, high order, high spatial resolution, ice sheet modeling using the Ice Sheet System Model (ISSM). *Journal of Geophysical Research: Earth Surface* **117** (1), 1–20.

Lipovsky BP and Dunham EM (2017) Slow-slip events on the Whillans Ice Plain, Antarctica, described using rate-and-state friction as an ice stream sliding law. *Journal of Geophysical Research: Earth Surface* **122**(4), 973–1003.

Luthra T and 5 others (2017) Characteristics of the sticky spot of Kamb Ice Stream, West Antarctica. *Journal of Geophysical Research: Earth Surface* **112**(3), 641–653.

Luthra T, Anandakrishnan S, Winberry JP, Alley RB and Holschuh N (2016) Basal characteristics of the main sticky spot on the ice plain of Whillans Ice Stream, Antarctica. *Earth and Planetary Science Letters* **440**, 12–19.

MacAyeal DR (1989) Large-scale ice flow over a viscous basal sediment: theory and application to Ice Stream B, Antarctica. *Journal of Geophysical Research: Solid Earth* **94**(B4), 4071–4087.

MacAyeal DR, Bindschadler RA and Scambos TA (1995) Basal friction of Ice Stream E, West Antarctica. *Journal of Glaciology* **41**(138), 247–262.

Macgregor JA and 6 others (2016) Holocene deceleration of the Greenland Ice Sheet. *Science (New York, N.Y.)* **351**(6273), 590–593.

Morland L (1987) Unconfined ice-shelf flow. In Dynamics of the West Antarctic Ice Sheet: Proceedings of a Workshop Held in Utrecht, May 6–8, 1985. Springer, pp. 99–116.

Nereson N, Raymond C, Waddington E and Jacobel R (1998) Migration of the Siple Dome ice divide, West Antarctica. *Journal of Glaciology* **44**(148), 643–652.

Ng F and Conway H (2004) Fast-flow signature in the stagnated Kamb Ice Stream, West Antarctica. *Geology* **32**(6), 481–484.

Paden J, Li J, Leuschen C, Rodriguez-Morales F and Hale R (2014, updated 2019) *Icebridge MCoRDS L1B geolocated radar echo strength profiles, Version 2.* Boulder, CO, USA: National Snow and Ice Data Center.

Pattyn F (2003) A new three-dimensional higher-order thermomechanical ice sheet model: basic sensitivity, ice stream development, and ice flow across subglacial lakes. *Journal of Geophysical Research: Solid Earth* **108**(B8), 1–15.

Pattyn F and 20 others (2008) Benchmark experiments for higher-order and full-Stokes ice sheet models (ISMIP-HOM). *The Cryosphere* **2**, 95–108.

Price SF, Bindschadler RA, Hulbe CL and Blankenship DD (2002) Force balance along an inland tributary and onset to Ice Stream D, West Antarctica. *Journal of Glaciology* **48**(160), 20–30.

Raymond CF (1983) Deformation in the vicinity of ice divides. *Journal of Glaciology* **29**(103), 357–373.

Raymond C (1996) Shear margins in glaciers and ice sheets. *Journal of Glaciology* **42**(140), 90–102.

Rignot E and 5 others (2019) Four decades of Antarctic ice sheet mass balance from 1979–2017. *Proceedings of the National Academy of Sciences* **116**(4), 1095–1103.

Rignot E, Mouginot J and Scheuchl B (2011) Ice flow of the Antarctic Ice Sheet. *Science (New York, N.Y.)* **333**, 1427–1431.

Rignot E, Mouginot J and Scheuchl B (2017) *Measures InSAR-based Antarctica ice velocity map, Version 2.* Boulder, CO, USA: National Snow and Ice Data Center.

Roberts JL, Warner RC and Treverrow A (2013) Inferring ice-flow directions from single ice-sheet surface images using the radon transform. *Journal of Glaciology* **59**(213), 129–136.

Scambos T, Haran T, Fahnestock M, Painter T and Bohlander J (2007) MODIS-based mosaic of Antarctica (MOA) data sets: continent-wide surface morphology and snow grain size. *Remote Sensing of Environment* **111**(2–3), 242–257.

Sergienko OV and Hulbe CL (2011) 'Sticky spots' and subglacial lakes under ice streams of the Siple Coast, Antarctica. *Annals of Glaciology* **52**(58), 18–22.

Shi L and 8 others (2010) Multichannel coherent radar depth sounder for NASA Operation Ice Bridge. In 2010 IEEE International Geoscience and Remote Sensing Symposium, Honolulu, Hawaii, USA. IEEE, pp. 1729–1732.

Siegert M, Ross N, Corr H, Kingslake J and Hindmarsh R (2013) Late Holocene ice-flow reconfiguration in the Weddell Sea sector of West Antarctica. *Quaternary Science Reviews* **78**, 98–107.

Stokes CR, Clark CD, Lian OB and Tulaczyk S (2007) Ice stream sticky spots: a review of their identification and influence beneath contemporary and palaeo-ice streams. *Earth-Science Reviews* **81**(3–4), 217–249.

Tulaczyk S, Kamb WB and Engelhardt HF (2000) Basal mechanics of Ice Stream B, west Antarctica: 2. Undrained plastic bed model. *Journal of Geophysical Research* **105**(1999), 483.

Vaughan DG, Corr HF, Doake CS and Waddington ED (1999) Distortion of isochronous layers in ice revealed by ground-penetrating radar. *Nature* **398**(6725), 323.

Vieli GML, Hindmarsh RC and Siegert MJ (2007) Three-dimensional flow influences on radar layer stratigraphy. *Annals of Glaciology* **46**, 22–28.

Winberry JP, Anandakrishnan S, Wiens DA, Alley RB and Christianson K (2011) Dynamics of stick–slip motion, Whillans Ice Stream, Antarctica. *Earth and Planetary Science Letters* **305**(3–4), 283–289.

Winter K and 6 others (2015) Airborne radar evidence for tributary flow switching in Institute Ice Stream, West Antarctica: Implications for ice sheet configuration and dynamics. *Journal of Geophysical Research: Earth Surface* **120**, 1611–1625.

Wolovick MJ and Creyts TT (2016) Overturned folds in ice sheets: insights from a kinematic model of traveling sticky patches and comparisons with observations. *Journal of Geophysical Research: Earth Surface* **121**(5), 1065–1083.

Wolovick MJ, Creyts TT, Buck WR and Bell RE (2014) Traveling slippery patches produce thickness-scale folds in ice sheets. *Geophysical Research Letters* **41**(24), 8895–8901.

Young TJ and 8 others (2018) Resolving the internal and basal geometry of ice masses using imaging phase-sensitive radar. *Journal of Glaciology* **64**(246), 649–660.